Chinese Chemical Letters 33 (2022) 2165–2170

Contents lists available at ScienceDirect

Chinese Chemical Letters

journal homepage: www.elsevier.com/locate/cclet

# Interwoven nickel(II)-dimethylglyoxime nanowires in 3D nickel foam for dendrite-free lithium deposition

Tianyi Zhou[a,c], Yanlu Mu[a,c], Jianyang Wu[b], Bing Zhong[c], Chengkai Yang[e], Qian Wang[f], Wen Liu[d,*], Henghui Zhou[b,*], Peng Jiang[a,c,*]

[a] CAS Key Laboratory of Standardization and Measurement for Nanotechnology, CAS Center for Excellence in Nanoscience, National Center for Nanoscience and Technology, Beijing 100190, China
[b] College of Chemistry and Molecular Engineering, Peking University, Beijing 100871, China
[c] University of Chinese Academy of Sciences, Beijing 100049, China
[d] State Key Laboratory of Chemical Resource Engineering, College of Chemistry, Beijing Advanced Innovation Center for Soft Matter Science and Engineering, Beijing University of Chemical Technology, Beijing 100029, China
[e] College of Materials Science and Engineering, Fuzhou University, Fuzhou 350108, China
[f] Institute of Energy Innovation, College of Materials Science and Engineering, Taiyuan University of Technology, Taiyuan 030024, China

ARTICLE INFO

*Article history:*
Received 3 September 2021
Revised 14 October 2021
Accepted 19 October 2021
Available online 26 October 2021

*Keywords:*
Nickel(II)-dimethylglyoxime
Nickel foam
Metal-organic complex
Uniform nucleation
Dendrite-free

ABSTRACT

Metal skeletons, such as Nickel Foam (NF) has attracted worldwide interests as stable host for lithium metal anode because of its high stability, large specific surface area and high conductivity. However, most metal skeletons have lithophobic surface and uneven current distribution that result in sporadic lithium nucleation and uncontrolled dendrites growth. Herein, we describe a sequential immersing strategy to generate interwoven Nickel(II)-dimethylglyoxime (Ni-DMG) nanowires at NF to obtain composite skeleton (NDNF), which can be used as an stable host for Li metal storage. The Ni-DMG has proved effective to realize uniform lithium nucleation and dendrite-free lithium deposition. Combing with the three dimensional (3D) hierarchical porous structure, the composite host shows a significantly improved coulombic efficiency (CE) than pristine commercial nickel foam. Moreover, the corresponding Li||Li symmetrical cells can run more than 700 h with low voltage hysteresis 22 mV at 1.0 mA/cm$^2$, and Li@NDNF||$LiFePO_4$ full-cell exhibits a high capacity retention of 82.03% at 1.0 C during 630 cycles. These results proved the effectiveness of metal-organic complexes in governing Li metal growth and can be employed as a new strategy for dendrite-free Li metal anode and safe Li metal batteries (LMBs).



Lithium metal is widely considered as an ideal candidate anode material for high energy density secondary battery systems such as lithium sulfur (≈ 650 Wh/kg), lithium air (≈ 950 Wh/kg) and solid lithium metal batteries [1,2], owing to its excellent electrochemical properties such as the lowest electrochemical potential (−3.04 V *vs.* the standard hydrogen electrode), high theoretical specific capacity (3860 mAh/g), and low density (0.59 g/cm$^3$) [3,4]. Unfortunately, two formidable challenges still impede practical or commercial applications of lithium metal anode. On one hand, inhomogeneous lithium nucleation in the electrochemical process leads to severe lithium dendritic growth that cause huge volume change and result in safety problems such as short circuit [5,6]. On the other hand, the repetitive crack and formation of solid electrolyte interphase (SEI) film consume consistently both lithium anode and electrolyte along with generating "dead Li", which produces as result reduced coulombic efficiency (CE) [7,8].

For decades, massive efforts have been made to find solutions to overcome these challenges, such as constructing artificial protective layers [9–11], adjusting electrolyte composition [12–15] and designing of solid state electrolyte [16,17]. According to the Sand's time model [18,19], lowering the effective current density *via* the design of three-dimensional (3D) current collectors is another effective method for suppressing Li dendrites growth [20–22]. Several applicable materials such as carbon hosts [23–25], organic structure, [26,27] 3D metal skeletons [28,29] have been reported to be used in approaches based on Sand's time model. The commercial metal foams, such like Ni Foam (NF) and copper foam, due to their excellent structural integrity and electrical conductivity, have been widely employed as both the supporting substrate and current collector for electrochemical applications [30].

* Corresponding authors.
*E-mail addresses:* wenliu@mail.buct.edu.cn (W. Liu), hhzhou@pku.edu.cn (H. Zhou), pjiang@nanoctr.cn (P. Jiang).

https://doi.org/10.1016/j.cclet.2021.10.051
1001-8417/

Problems still remain in these approaches with metal skeletons (Ni, Cu, Al) being used as current collector: the large pore size, uneven distribution of current on the surface of the skeleton and large nucleation potential barrier caused by the lack of lithiophilicity, lead to the growth of lithium dendrites and the formation of dead lithium [31]. Thus, surface modification of the skeletons is desired to reduce the nucleation over-potential during the initial stage in order to realize uniform Li nucleation. Besides precious metals [32], metal oxides [33–35], metal nitrides [36] and N-doped carbon [37,38], materials such as metal organic frameworks (MOFs) with functional groups [39–41] proved to have strong affinity to lithium and were used for surface modification of metal skeletons to achieve uniform lithium deposition [42]. In addition, an emerging strategy has also been reported that the elastic polymers are filled into the host pores to generate self-adaptable pressure to achieve uniform Li plating/stripping with a high utilization [43]. However, these approaches are either too expensive, and/or require a complicated synthesis procedure. Therefore, finding a low cost, facile and scalable method to make three-dimensional current collector as well as the stable lithium metal host is the key problem to improve the electrochemical performance of lithium metal anode.

In this work, surface-modified current collectors (NDNF) were fabricated through *in-situ* growth of nickel(II)-dimethylglyoxime (Ni-DMG) on Ni foam (NF). Ni-DMG is a stable metal-organic complex composed of dimethylglyoxime and nickel ions [44–47]. Outcomes proved that Ni-DMG modified skeleton exhibited strong affinity to Li ions, which enabled a homogeneous Li nucleation during initial stage, then the dendrite-free Li deposition in the following process. The nucleation over-potential at initial stage has been significantly and effectively reduced. In consequence, the Li@NDNF||Li@NDNF symmetrical cells displayed a stable cycling performance with low and stable voltage hysteresis of 22 mV at 1.0 mA/cm$^2$ and with capacity of 1.0 mAh/cm$^2$ over 700 h. The Li@NDNF||$LiFePO_4$ full-cell maintains a stable cycling at 1.0 C with high capacity retention of 82.03% in 630 cycles. Therefore, this facile strategy shed a new light on solving the problems of dendrites growth of Li metal anode, making it a feasible choice for the practical application of LMBs.

50 mg dimethylglyoxime (DMG) was dissolved in 10 mL ethanol (Sol.1) and 50 mg $Ni(NO_3)_2$ was dissolved in 10 mL ethanol (Sol.2). Sol.1 to Sol.2 were mixed to prepare pure Ni-DMG. The obtained Ni-DMG was washed by ethanol and then dried in air at 90 °C for minutes to evaporate ethanol. The preparation of Ni-DMG follow this formula [44]:

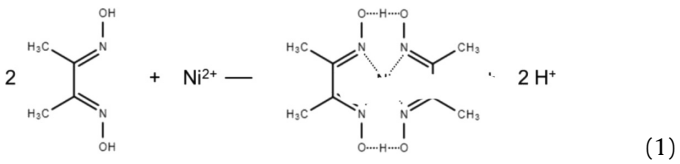


(1)

To prepare surface lithiophilic three dimensional current collector, commercial Ni foam (NF) was cut into tablets with size suitable for coin cells (CR2032) assembling. Firstly, NF was immersed in Sol.1 for 10 s to let $Ni^{2+}$ adsorbed onto NF skeleton. After air dried for 1 min, above NF was immersed into Sol.2 to generate the Ni-DMG on NF and was then taken out immediately. The NF was air dried again for 1 min, then washed by ethanol and dried in air at 90 °C. The obtain nickel foam was interwove with Ni-DMG, and named as nickel(II)-dimethylglyoxime@nickle foam (NDNF). The thickness of interwoven Ni-DMG nanowires on the surface of NDNF is about 3∼4 μm. And the average mass of Ni-DMG on NDNF is about 0.39 mg/cm$^2$. The thickness of NDNF host is the same with that of NF host, is 0.621 mm (Fig. S1 in Supporting information).

The morphology of different samples was observed by the field emission scanning electron microscope (SEM, Hitachi S4800) operated at 10 kV. The PANalytical diffractometer with Cu K$\alpha$ radiation was employed to obtain Powder X-ray diffraction (XRD) data. X-ray photoelectron spectrums (XPS) were recorded on an Imaging Photoelectron Spectrometer (Kratos Analytical Ltd.) and the binding energies were referenced to the C 1s peak at 284.8 eV of the surface adventitious carbon.

To evaluate the electrochemical performance of NDNF, CR2032-type coin cells were assembled in the glove box filled with Ar gas ($H_2O$ < 0.1 ppm, $O_2$ < 0.1 ppm). These coin cells were then tested on battery testing system (Land battery tester, Wuhan, China) at room temperature (25 °C). Two different electrolytes were used: The ether electrolyte was prepared by introducing 1.0 mol/L LiTFSI into DOL and DME (1:1, v/v) with 2.0 wt% $LiNO_3$ addition; the ester electrolyte (1.0 mol/L $LiPF_6$ in EC + DMC + EMC + DEC + ads) was purchased from Shanghai Xiaoyuan Energy Technology Co., Ltd.

For symmetrical cell test, lithium metal of 10 mAh/cm$^2$ was plated into each skeletons (NF and NDNF) by electrochemical method. Then two as-prepared Li plated electrodes (Li@NDNF or Li@NF) were assembled into one coin cell with ether electrolyte.

For full-cells evaluation, ester electrolyte was used. $LiFePO_4$ (LFP, Pulead Co., Ltd.), carbon black and PVDF were mixed in *N*-methylpyrrolidone (NMP) with a weight ratio of 8:1:1 to form a slurry; and then, this slurry was coated on Al foil and dried under vacuum to prepare the LFP cathode. $LiNi_{0.8}Co_{0.1}Mn_{0.1}O_2$ (NCM811, Pulead, Co., Ltd.), carbon black and poly(1,1-difluoroethylene) (PVDF) was also mixed in NMP (8:1:1), coated on Al foil and dried under vacuum to prepare the NCM811 cathode. Finally, the cathode was paired with Li@NDNF or Li@NF anodes to assemble coin cells, with usage of ester electrolyte. The active material loading of the LFP or NCM811 cathode is controlled at 8 mg/cm$^2$ (∼1.3 mAh/cm$^2$ for LFP and ∼1.6 mAh/cm$^2$ for NCM811, respectively) and the amount of lithium in both two anodes is 20.0 mAh/cm$^2$ (∼825 mAh/g for Li@NDNF or Li@NF). The active material loading of the high areal mass loading LFP cathode is controlled at 16 mg/cm$^2$ (∼2.6 mAh/cm$^2$). The active material loading of the high areal mass loading NCM811 cathode is controlled at 24 mg/cm$^2$ (∼4.8 mAh/cm$^2$). The full-cells with LFP cathode was tested in the potential range of 2.5–4.1 V *vs.* $Li^+$/Li, and the full-cells with NCM811 cathode was tested in the potential range of 2.5–4.25 V *vs.* $Li^+$ /Li.

The cyclic voltammetry test (CV) was carried out *via* Li||NF and Li||NDNF coin cells at the scan rate of 10 mV/s. The electrochemical impedance spectroscopy (EIS) of the symmetrical cells was conducted in the frequency range of 0.01 Hz to 100 kHz.

Figs. 1a and b show the schematics of the NDNF synthesized through sequential immersing treatment. Ni foam (NF) was immersed in $Ni^{2+}$ and DMG solution in order, forming the interwoven Ni-DMG nanowires. The whole treatment process is so easy that can be finished in minutes. After sequential immersing treatment, the color of NF turned from silvery with metallic-luster to dark red, meaning the Ni-DMG was successfully generated on NF. From SEM image in Fig. 1c, we can observe that the inner surface of pristine NF was smooth. After surface decoration, abundant of Ni-DMG nanowires is tightly coated on the surface of NF substrate and interwove like spider webs (Fig. 1d). The thickness of this Ni-DMG modified layer can be controlled by adjusting the concentration of $Ni(NO_3)_2$ and dimethylglyoxime (DMG) solution (Fig. S2 in Supporting information).

X-ray photoelectron spectroscopy (XPS) was then carried out to probe the surface chemistry of NDNF (Figs. 2a and b). The XPS Ni 2p peaks can be divided into two different peaks. The peaks at 852.3 eV and 870.0 eV can be assigned to Ni(0) [48,49]. The peaks near 854.0 eV and the peak at 871.8 eV are attributed to Ni(II), and

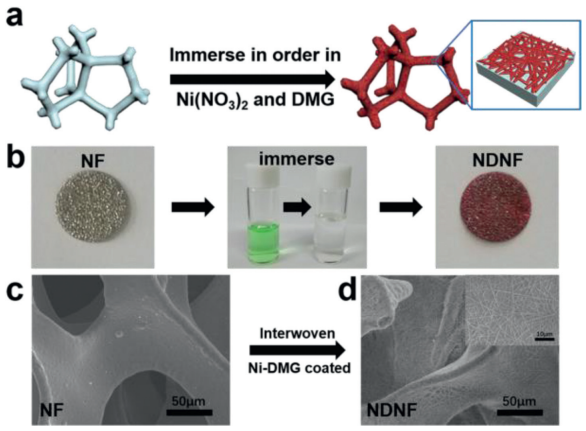


**Fig. 1.** The schematics of the fabrication process of NDNF. (a) The schematics and (b) the optical images of the fabrication process of NDNF and corresponding optical image of each step. The SEM images of (c) NF and (d) NDNF.

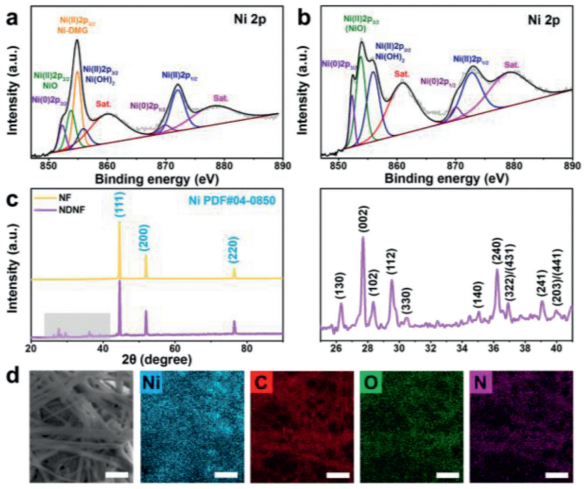


**Fig. 2.** The characterization of NDNF. The XPS spectrum for Ni 2p of (a) NDNF and (b) NF. (c) The XRD pattern of NF and NDNF, and the enlarged view of the gray area. (d) The SEM image of NDNF and the corresponding elements mapping of it (The scale bar in these figures are 1 μm).

the peaks at 860.4 and 879.1 eV are attributed to satellite peaks of Ni(II) [50]. There are three kind of Ni(II) compounds that can be identified from the spectra of NDNF surface, which are NiO, Ni-DMG and NiOH, corresponding to the peaks at 853.9 eV [51], 854.9 eV [52] and 855.9 eV [53]. The above results indicated that sequential immersing treatment could produce a uniform layer of interwoven Ni-DMG on the pristine nickel foam. On the contrary, the XPS spectra of pristine NF show no corresponding peak of Ni-DMG.

In the X-ray diffraction (XRD) patterns of NF and NDNF are exhibited in Fig. 2c. There are three strong peaks at 44.507°, 51.846° and 76.370°, which perfectly match the standard patterns of Ni (PDF#04–0850). Besides the peaks of Ni, the XRD pattern of NDNF shows other small peaks from 25° to 41°, which can be attributed to the Ni-DMG, indicating again that the product of treatment is Ni-DMG crystal [54,55]. The pure Ni-DMG was fabricated *via* same wet-method, and then was analyzed by XRD for comparison (Fig. S3 in Supporting information). From 25° to 41°, the XRD pattern of pure Ni-DMG shows characteristic peaks at the same position as the pattern of NDNF.

The detailed morphology and components of Ni-DMG on the NF surface can be seen from the SEM image and corresponding elemental mapping. Since a single Ni-DMG molecule has a structure of flake and the surface free energy of it is very high, so that the flake molecules are easy to stack along the c axis to form crystals, while the growth in the a and b axis directions is relatively slow [56]. Therefore, Ni-DMG crystal is easy to grow as nano-rod, as shown in Fig. S4 (Supporting information). In a short time of sequential immersing treatment, Ni-DMG grew into wire-like morphology with the diameter of only ~320 nm (Fig. S5 in Supporting information). The corresponding elements mapping exhibited in Fig. 2d revealed the distribution of Ni, C, O and N sites on the Ni-DMG nanowires in Ni foam. Although the signal of Ni was confused by the NF substrate, it can be observed that the Ni sites and C, O, N sites uniformly distributed in Ni-DMG complex and these Ni-DMGs evenly covered the surface of the NF substrate. These homogenous-covered Ni-DMGs would provide abundant of nucleation sites for Li metal.

The lithium deposition behavior was investigated under charge/discharge states during one whole cycle, as shown in Fig. 3, to illustrate the nucleation regulating *via* Ni-DMG. During the initial lithium plating states, the lithiation of Ni-DMG happened when Li ion inserted into the Ni-DMG (Fig. S6 in Supporting information), and then Li nucleated wrapping the Ni-DMG nanowires homogeneously (Fig. 3a). It is obvious that the lithium was deposited onto the material. In addition, as the deposition progressed, the parts of cavities of interwoven Ni-DMG and Ni skeletons were submerged by fresh-deposited lithium metal. Along with the proceeding of the deposition, lithium metal uniformly coated the Ni skeletons. In this structure, the NF played as electron conductor, providing electrons for lithium ions nucleation. While interwoven Ni-DMG above not only played the role of substrate with improved Li affinity to realize homogeneous $Li^+$ flux near the electrode surface by oxime groups, but also achieve further volume restriction of fresh-deposited lithium metal *via* its interwoven structure. Due to that, the NDNF exhibited a uniform dendrite-free Li deposition on entire Ni skeletons as the plating capacity increased from 1.0 mAh/cm$^2$ to 5.0 mAh/cm$^2$. (Figs. 3b-d) Just the reverse, the Li deposition on pristine NF showed sporadic nucleation and dendritic growth, as shown in Fig. S7 (Supporting information). A large amount of lithium nucleated on only a part of NF skeletons surface and grew as dendrites, while there is little lithium deposition on other parts. As a result, the lithium only deposited on the upper Ni skeletons of pristine NF, and there is no lithium deposition on the deep skeletons. Such an uneven deposition of Li metal on pristine NF leads to an extremely low utilization of the NF skeleton, and results in huge difficulty to inhibit the growth of dendrites. In addition, as the amount of deposition increases from 1.0 mAh/cm$^2$ to 5.0 mAh/cm$^2$, uneven deposition and dendritic growth of Li metal become more obvious.

During the subsequent charging process, lithium metal was stripped from the NDNF (Figs. 3e and f). The metal lithium deposited uniformly on the NDNF skeleton is gradually stripped off, re-exposing the Ni-DMG nanowires. During further stripping, even if most of the lithium is stripped away, the interwoven Ni-DMG nanowires can still remain stable. On contrast, the metal lithium deposited on the pristine NF show a terrible morphology after different amount of Li stripping (Fig. S8 in Supporting information). Lithium dendrites become sharper after Li stripping and these Li dendrites appeared to be broken. Therefore, a large amount of dead lithium is produced on the surface of NF, which is the main reason for the low coulombic efficiency (CE).

In order to explore the mechanism of uniform lithium deposition on NDNF, the nucleation over-potential of Li metal on the pristine NF and NDNF at a current density of 1.0 mA/cm$^2$ were investigated. The difference between the voltage tip and the stable voltage platform was defined as the value of the nucleation overpotential, which reflects the energy barrier of heterogeneous nucleation during the initial process. For pristine NF, Li directly nucleate and grow on its surface below 0 V (*vs.* $Li^+$/Li). The Li nucle-

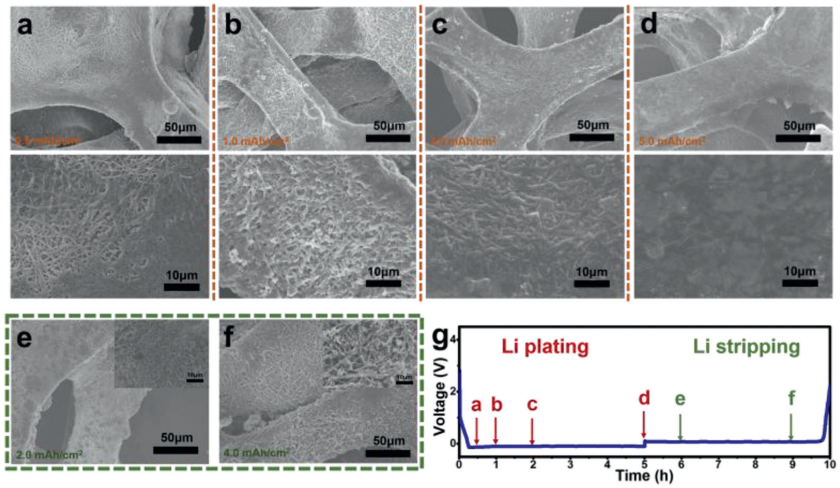


**Fig. 3.** The morphology evolution of lithium metal on NDNF during plating/stripping process. (a-d) The SEM images of NDNFs after Li plating with different area capacities at 1.0 mA/cm$^2$ and then (e, f) stripping with different area capacities at 1.0 mA/cm$^2$. The states of Li plating/stripping (a-f) are marked in (g) the galvanostatic discharge/charge voltage profile of a Li||NDNF half-cell.

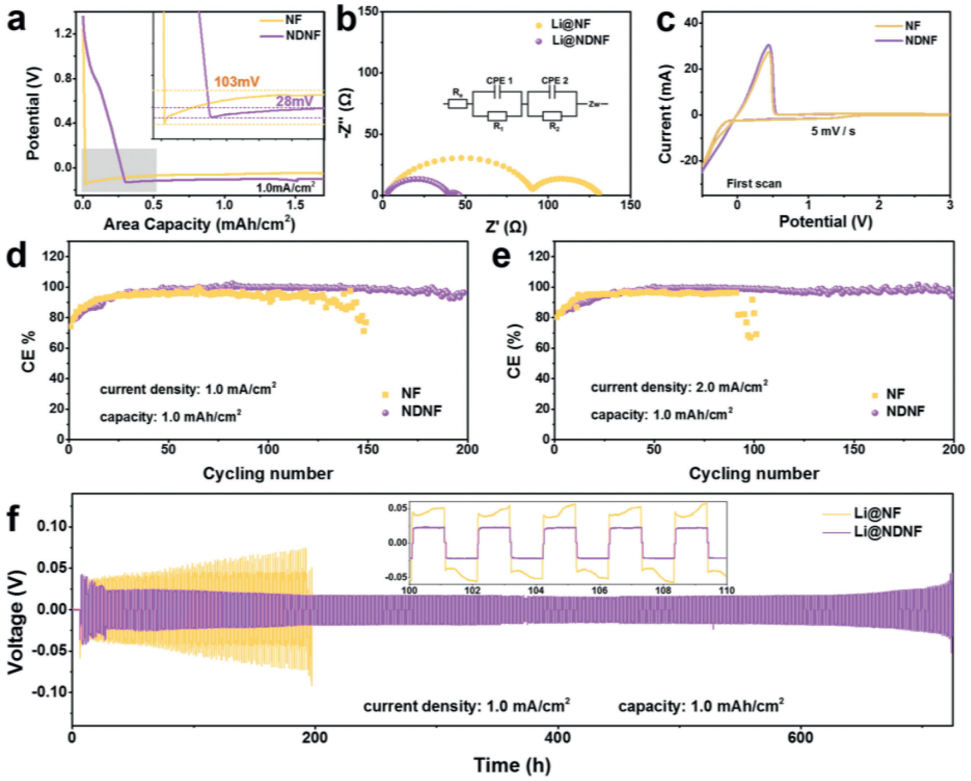


**Fig. 4.** Electrochemical analysis of NDNF. (a) The over-potential Li metal deposit on NF and NDNF (insert: enlarged view of nucleation over-potential comparison). (b) Nyquist plots of electrochemical impedance spectroscopy of symmetrical cells with Ni foam or NDNF that has 5.0 mAh/cm$^2$ of Li metal deposited on it. (c) Cyclic voltammetry curves of Li||Ni half-cells with NF or NDNF as counter electrode. The CE of Li||Ni half-cells at (d) 1.0 mA/cm$^2$, 1.0 mAh/cm$^2$ and (e) 2.0 mA/cm$^2$, 1.0 mAh/cm$^2$ with NF and NDNF as counter electrode. (f) The cycling performance of Li||Li symmetrical cells at 1.0 mA/cm$^2$, 1.0 mAh/cm$^2$. Insert detailed analysis of voltage profiles.

ation over-potential of the pristine NF is 103 mV, which indicate there is a high energy barrier of Li nucleation on NF need to overcome during Li deposition. In comparison, Li deposition on NDNF shows different voltage profile. $Li^+$ ions can be inserted into Ni-DMG and lithiated it below 1.0 V (*vs.* $Li^+$/Li), and then nucleate and grow on the modified surface below 0 V (*vs.* $Li^+$/Li). The Li deposition on NDNF exhibits smaller nucleation over-potential. The Li nucleation over-potential on NDNF is only 28 mV, demonstrating that the surface modification through the introduction of Ni-DMG nanowires on NF significantly improves the Li affinity of the Ni skeleton through the oxime groups (Fig. 4a). Finally, Li gradually deposits and fills the interspace between Ni-DMG nanowires on NDNF with the increase of Li deposition capacity, which corresponding with the lithium deposition behavior we mentioned before.

The high interfacial stability of the Li@NDNF anode compared to the Li@NF anode has also been verified by electrochemical impedance spectroscopy (EIS) measurements. Fig. 4b shows the Nyquist plots of the symmetrical cells with two kind anodes. As a result of uneven deposition and dendritic growth of Li metal on NF, the Li@NF anode shows a high interfacial resistance of 90.7 Ω. The Li@NDNF anode displays a low interfacial resistance of 39.8 Ω,

due to the uniform deposition on NDNF realizing an interface with lower energy barrier.

Electrochemical cyclic voltammetry (CV) tested in Li||NF and Li||NDNF half-cells were also employed to investigate the Li plating/stripping behaviors on NF and NDNF. In the first scan cycle (Fig. 4c), the potential of Li redox on NDNF was 0.434 V, which was lower than that on NF (0.441 V). In addition, the NDNF exhibited a higher peak current of 30.49 mA/cm$^2$ than that of NF (27.52 mA/cm$^2$). After four scan cycles, the CV curves of Li||NF and Li||NDNF preformed larger differences. Li||NDNF exhibited the redox potential of 0.353 V and the peak current of 31.08 mA/cm$^2$, whereas the redox potential of Li||NDNF is higher (0.366 mV) and the peak current (26.66 mA/cm$^2$) is smaller, clarified that a better electrochemical kinetics of Li redox can be achieved on the NDNF with Ni-DMG (Fig. S9 in Supporting information).

The CE of repeated Li plating/stripping on NF and NDNF were assessed *via* the Li||NF and Li||NDNF half-cells with a fixed capacity of 1.0 mAh/cm$^2$ were performed at various current densities. As shown in Fig. 4d, the Li||NDNF half-cell kept a stable CE of ~97.24% throughout 200 cycles at a current density of 1.0 mA/cm$^2$. While the CE of Li||NF dropt to below 80% after ~150 cycles and then fluctuated randomly, attributing to the "dead Li" and the repeated formation/facture of SEI. Moreover, the average CE of Li||NDNF remained stable at ~97.04% at 2.0 mA/cm$^2$ during 200 cycles, while the Li||NF half-cell can remain stable CE of ~93.6% for 100 cycles and then severely fluctuated (Fig. 4e). Notably, when the current density raised up to 5.0 mA/cm$^2$, the Li plating/stripping on NDNF can still maintain the average CE of ~94.94% during 200 cycles. In contrast, the stable CE of the Li||NF half-cell only lasted for fewer cycles and fluctuated more severely to failure, which could be attributed to inner short-circuit due to Li dendrites (Fig. S10 in Supporting information). The CE of repeated Li plating/stripping on NF and NDNF with a fixed current density of 1.0 mA/cm$^2$ at different capacities of 2.0 and 3.0 mAh/cm$^2$ were also performed, as shown in Fig. S11 (Supporting information)**.** It can be observe that the Li||NDNF half-cell can cycle with average CE over 90%, while Li||NF exhibit lower average CE about only 80% and short circuit quickly.

The Li||Li symmetrical cells was investigated to compare the galvanostatic cycling performance of NF and NDNF at 1.0 mA/cm$^2$, as shown in Fig. 4f. Before the test, 10 mAh/cm$^2$ of lithium was deposited onto the NF and NDNF at 1.0 mA/cm$^2$ to fabricate the Li@NF and Li@NDNF anodes. Due to the lithium dendritic growth, formation of "dead Li" and the repeated formation/facture of SEI during cycling process, the Li@NF||Li@NF symmetrical cells showed substantial voltage increasing as the cycle going on. A larger voltage hysteresis over 40 mV can be observed just at beginning of cycling, and then it kept increasing over 50 mV. The sharp voltage drop of Li@NF||Li@NF symmetrical cells at 200 h indicated the happening of short-circuit. However, the symmetrical cells assembled with Li@NDNF performed flat voltage hysteresis over 700 h. From the detailed comparison shown in the insets of Fig. 4f, the over-potential of Li@NF||Li@NF cell kept high (52 mV) and frequent voltage fluctuation was observed. On the contrary, stable over-potential of 22 mV can be maintained with Li@NDNF as electrode.

To investigate the stability of NDNF during repeated Li plating/stripping process, The XPS was employed again (Fig. S12 in Supporting information). From the comparison of Li@NF and Li@NDNF after 20 cycles at 1.0 mA/cm$^2$, the peak at 854.9 eV of Ni-DMG still obvious, indicating that the interwoven Ni-DMG nanowires can maintain stable during cycling.

The morphologies of the cycled Li@NF and Li@NDNF anode with different amount of Li metal deposited at 1.0 mA/cm$^2$ on it were investigated *via* SEM. With 5.0 mAh/cm$^2$ of lithium deposited, the Li@NF anode showed uneven surface with a great amount of loose packed Li dendrites and "dead Li" after cycled 20 cycles at 1.0 mA/cm$^2$, 1.0 mAh/cm$^2$, whereas the cycled Li@NDNF anode exhibited dense and smooth surface, as shown in Figs. S13a and c (Supporting information). At the high plating capacity of 10.0 mAh/cm$^2$, the cycling performance of Li@NF is the same terrible. The deposited metal lithium is separated from the skeleton of the pristine NF, which is due to the poor affinity of the NF surface with lithium. Different from Li@NF, the Li@NDNF exhibited a uniform and dense deposition of lithium without any dendrites and "dead Li". The morphology comparison after repeated plating/stripping illustrated that the Ni-DMG modified NF (NDNF) can lead to effectively homogenize the nucleation of Li metal and keep structure stable during cycling (Figs. S13b and d in Supporting information).

To demonstrate the potential of practical application of Li@NDNF anode, the cycling performance of Li@NF and Li@NDNF anode in full-cell with $LiFePO_4$ (LFP) or NCM811 as the cathode was tested. The long-term cycling performance at 1.0 C of full-cells with LFP as cathode were shown in Fig. 5a. The CE of Li@NF||LFP full-cell fluctuated and then decreased when it run for less than 50 cycles, not only because the lithium metal fall off from NF skeleton and formed "dead Li" due to the poor affinity with lithium of NF, but also as a result of uneven deposition surface leading to repeated formation/facture of SEI. After 290 cycles, the specific capacity and CE of Li@NF||LFP full-cell exhibited a sharp decay due to the internal short-circuit. However, the Li@NF||LFP full-cell performed a stable cycling (stable CE of 99.33%) as well as the discharge capacity retention of more than 82.03% after 630 cycles. The charge and discharge curves of two full-cells at 1.0 C were displayed in Fig. 5b and the Li@NDNF||LFP full-cell exhibited the flat voltage plateau with lower polarization revealing that Li@NDNF had a better electrochemical kinetic than Li@NF. As demonstrated in Fig. 5c, the values of specific capacity of Li@NF||LFP full-cell dropt dramatically as the C-rate raised up from 1.0 C to 10.0 C. However, for Li@NDNF||LFP full-cell, the specific capacity can remain a higher value than that of Li@NF||LFP full-cell even at high C-rates. Beside, when the C-rate returned to 1.0 C, the specific capacity of full-cell using Li@NDNF anode can recover well due to its high reversibility. The morphology of Li@NF and Li@NDNF anode cycled in full-cell after 50 cycles was investigated, as shown in Figs. 5d and e. It is obvious that a dendrite-free surface was achieved on the Li@NDNF instead of the Li@NF. The full-cells with NCM811 cathode and Li@NDNF anode also displayed an improved cycling performance during 200 cycles, while the NCM811 full-cell with Li@NF anode suffered a short-circuit after less than 70 cycles (Fig. S14 in Supporting information). Furthermore, even matching with high areal mass loading LFP and NCM811 cathode, the full-cells with Li@NDNF anodes still exhibit improved cycling performance compared with the full-cells with Li@NF anodes (Fig. S15 in Supporting information).

In summary, a uniform modification layer consist of interwoven Ni-DMG nanowires has been introduced on the Ni foam skeleton by a facile sequential immersing strategy to address the inhomogeneous nucleation and dendritic growth issue of Li metal. During Li deposition process, the interwoven Ni-DMG can serve as an effective regulator to realized uniform Li nucleation and dendrite-free Li deposition on NDNF with the help of abundant oxime groups providing improved affinity to $Li^+$. In addition, the unique interwoven structure of covered Ni-DMG area can effectively prevent deposited Li fall of from NF surface. As a result, uniform Li nucleation and dendrite-free deposition can be achieved on NDNF. This strategy developed a promising avenue of using metal-organic complex materials to realize high-performance lithium metal anode.

## Declaration of competing interest

The authors declare that they have no known competing financial interests or personal relationships that could have appeared to influence the work reported in this paper.

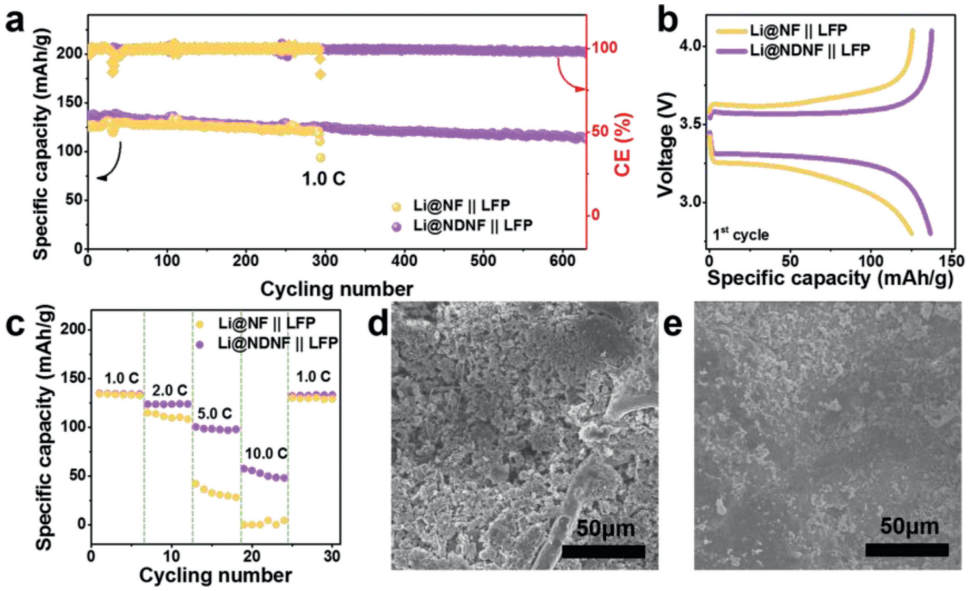


**Fig. 5.** Cycling performance. (a) The cycling performance of Li@NF||LFP and Li@NDNF||LFP full-cells at 1.0 C and (b) corresponding charge-discharge curves for the first cycle. (c) The rate performance of Li@NF||LFP and Li@NDNF||LFP full-cells. The SEM image of (d) Li@NF anode and (e) Li@NDNF anode from dis-assembled Li@NF||LFP and Li@NDNF||LFP full-cells after 50 cycles at 1.0 C, respectively.

## Acknowledgements

This work was financially supported by PULEAD Technology Industry Co., Ltd., the Strategic Priority Research Program of Chinese Academy of Sciences (No. XDB36000000), the National Key Research and Development Program of China (No. 2016YFA0200904), the National Natural Science Foundation of China (Nos. 21771018 and 21875004), the Natural Science Foundation of Beijing (No. 2192018), National Natural Science Foundation of China-Regional Innovation Joint Exploration Fund (No. U19A2019), and Beijing University of Chemical Technology (Start-up grant No. buctrc201901, BUCT, China).

## Supplementary materials

Supplementary material associated with this article can be found, in the online version, at doi:10.1016/j.cclet.2021.10.051.

## References

[1] E. Cha, M.D. Patel, J. Park, et al., Nat. Nanotechnol. 13 (2018) 337–344.
[2] X.G. Han, Y.H. Gong, K. Fu, et al., Nat. Mater. 16 (2017) 572–579.
[3] H. Kim, G. Jeong, Y.U. Kim, et al., Chem. Soc. Rev. 42 (2013) 9011–9034.
[4] W. Xu, J.L. Wang, F. Ding, et al., Energy Environ. Sci. 7 (2014) 513–537.
[5] R. Bhattacharyya, B. Key, H.L. Chen, et al., Nat. Mater. 9 (2010) 504–510.
[6] L.M. Suo, Y.S. Hu, H. Li, M. Armand, L.Q. Chen, Nat. Commun. 4 (2013) 9.
[7] B. Liu, J.G. Zhang, W. Xu, Joule 2 (2018) 833–845.
[8] M.D. Tikekar, S. Choudhury, Z.Y. Tu, L.A. Archer, Nat. Energy 1 (2016) 1–7.
[9] J.L. Lang, Y.Z. Long, J.L. Qu, et al., Energy Storage Mater. 16 (2019) 85–90.
[10] D.C. Lin, Y.Y. Liu, W. Chen, et al., Nano Lett. 17 (2017) 3731–3737.
[11] H. Wu, Q.P. Wu, F.L. Chu, et al., J. Power Sources 419 (2019) 72–81.
[12] X.D. Ren, S.R. Chen, H. Lee, et al., Chem 4 (2018) 1877–1892.
[13] H. Ota, K. Shima, M. Ue, J. Yamaki, Electrochim. Acta 49 (2004) 565–572.
[14] X.B. Cheng, R. Zhang, C.Z. Zhao, et al., Adv. Sci. 3 (2016) 20.
[15] K. Xu, Chem. Rev. 114 (2014) 11503–11618.
[16] S.Y. Li, W.P. Wang, S. Xin, J. Zhang, Y.G. Guo, Energy Storage Mater. 32 (2020) 458–464.
[17] F.P. Zhao, Q. Sun, C. Yu, et al., ACS Energy Lett. 5 (2020) 1035–1043.
[18] K. Wu, B.L. Zhao, C.K. Yang, et al., J. Energy Chem. 43 (2020) 16–23.
[19] L. Fan, S.Y. Li, L. Liu, et al., Adv. Energy Mater. 8 (2018) 8.
[20] R. Zhang, X.B. Cheng, C.Z. Zhao, et al., Adv. Mater. 28 (2016) 2155–2162.
[21] Y.L. Xu, A.S. Menon, P. Harks, et al., Energy Storage Mater. 12 (2018) 69–78.
[22] P. Shi, X.Q. Zhang, X. Shen, et al., Adv. Mater. Technol. 5 (2020) 15.
[23] L. Liu, Y.X. Yin, J.Y. Li, et al., Adv. Mater. 30 (2018) 8.
[24] R. Mukherjee, A.V. Thomas, D. Datta, et al., Nat. Commun. 5 (2014) 10.
[25] D.C. Lin, Y.Y. Liu, Z. Liang, et al., Nat. Nanotechnol. 11 (2016) 626–632.
[26] B.Q. Li, X.R. Chen, X. Chen, et al., Research 2019 (2019) 11.
[27] Y.W. Song, P. Shi, B.Q. Li, et al., Matter 4 (2021) 13.
[28] L.L. Lu, J. Ge, J.N. Yang, et al., Nano Lett. 16 (2016) 4431–4437.
[29] S.S. Chi, Y.C. Liu, W.L. Song, L.Z. Fan, Q. Zhang, Adv. Funct. Mater. 27 (2017) 10.
[30] X.B. Cheng, R. Zhang, C.Z. Zhao, Q. Zhang, Chem. Rev. 117 (2017) 10403–10473.
[31] Z.Y. Lu, Q.H. Liang, B. Wang, et al., Adv. Energy Mater. 9 (2019) 8.
[32] X. Ke, Y.H. Liang, L.H. Ou, et al., Energy Storage Mater. 23 (2019) 547–555.
[33] B.Z. Yu, T. Tao, S. Mateti, S.G. Lu, Y. Chen, Adv. Funct. Mater. 28 (2018) 9.
[34] X. Huang, X.Y. Feng, B. Zhang, et al., ACS Appl. Mater. Interfaces 11 (2019) 31824–31831.
[35] X.Y. Yue, W.W. Wang, Q.C. Wang, et al., Energy Storage Mater. 14 (2018) 335–344.
[36] J.F. Zhu, J. Chen, Y. Luo, et al., Energy Storage Mater. 23 (2019) 539–546.
[37] F.H. Ren, Z.Y. Lu, H. Zhang, et al., Adv. Funct. Mater. 28 (2018) 12.
[38] H.K. Kang, S.G. Woo, J.H. Kim, et al., J. Power Sources 413 (2019) 467–475.
[39] Y.C. Lin, Q.J. Zhang, C.C. Zhao, et al., Chem. Commun. 51 (2015) 697–699.
[40] X.X. Li, F.Y. Cheng, S.N. Zhang, J. Chen, J. Power Sources 160 (2006) 542–547.
[41] X.B. Lou, Y.Q. Ning, C. Li, et al., Sci. China Mater. 61 (2018) 1040–1048.
[42] D.M. Yin, Z.M. Wang, Q. Li, et al., iScience 23 (2020) 22.
[43] P. Shi, X.Q. Zhang, X. Shen, et al., Adv. Funct. Mater. 31 (2021) 7.
[44] S. Yamada, R. Tsuchida, J. Am. Chem. Soc. 75 (1953) 6351–6352.
[45] E. Booth, J.D.H. Strickland, J. Am. Chem. Soc. 75 (1953) 3017–3019.
[46] U. Muralikrishna, A. Sivaramakrishna, Asian J. Chem. 14 (2002) 1782–1784.
[47] T. Poltue, R. Rangkupan, S.T. Dubas, L. Dubas, Mater. Lett. 65 (2011) 2231–2234.
[48] P.T. Andrews, T. Collins, P. Weightman, J. Phys. C: Solid State Phys. 14 (1981) L957–L960.
[49] L.S. Hsu, R.S. Williams, J. Phys. Chem. Solids 55 (1994) 305–312.
[50] E.E. Khawaja, M.A. Salim, M.A. Khan, et al., J. Non-Cryst. Solids 110 (1989) 33–43.
[51] T. Dickinson, A.F. Povey, P.M.A. Sherwood, J. Chem. Soc. Faraday Trans. I 73 (1977) 327–343.
[52] T. Yoshida, K. Yamasaki, Bull. Chem. Soc. Jpn. 54 (1981) 935–936.
[53] L. Salvati, L.E. Makovsky, J.M. Stencel, F.R. Brown, D.M. Hercules, J. Phys. Chem. 85 (1981) 3700–3707.
[54] A.A. Dakhel, Y.A.M. Ahmed, F.Z. Henari, Opt. Mater. 28 (2006) 925–929.
[55] G. Hihara, M. Satoh, T. Uchida, F. Ohtsuki, H. Miyamae, Solid State Ion. 172 (2004) 221–223.
[56] D.X. Li, D.J. Xu, Y.Z. Xu, Acta Cryst. E 59 (2003) M1094–M1095.